IOP PUBLISHING JOURNAL OF PHYSICS D: APPLIED PHYSICS

J. Phys. D: Appl. Phys. **40** (2007) 5984–5994 doi:10.1088/0022-3727/40/19/031

Contact mechanics of layered elastic materials: experiment and theory

P M McGuiggan[1], J S Wallace[2], D T Smith[3,6], I Sridhar[4], Z W Zheng[4] and K L Johnson[5]

[1] Department of Materials Science and Engineering, Johns Hopkins University, Baltimore, MD 21218, USA
[2] MACS Consulting, Germantown, MD 20874, USA
[3] Ceramics Division, National Institute of Standards and Technology, 100 Bureau Drive, Gaithersburg, MD 20899, USA
[4] School of Mechanical and Aerospace Engineering, Nanyang Technological University, 50 Nanyang Avenue, Singapore 639798, Singapore
[5] Engineering Department, University of Cambridge, Trumpington Street, Cambridge, England CB2 1PZ, UK

Received 28 June 2007
Published 21 September 2007
Online at stacks.iop.org/JPhysD/40/5984

Abstract

This paper reports an experimental and theoretical investigation of the indentation of a layered elastic solid, with special reference to the surface force apparatus (SFA). The contacting surfaces of the SFA comprise a 3-layer material: a thin mica surface layer on a thicker epoxy layer supported by a thick silica substrate. An existing finite element analysis of the deformation of ideal mica/epoxy/silica surfaces used in the SFA is adapted to compare with the experimental measurements of the variation of contact size with load, both with and without adhesion at the interface. This is in marked difference to the Johnson, Kendall and Roberts (JKR) theory for homogeneous solids. Experiments and finite element calculations were also carried out on the elastic indentation of a thin (5.5 μm) layer of mica on a very thick layer of epoxy (>100 μm). As input data for the calculations, the elastic moduli of the mica and epoxy were measured in separate indentation experiments. The stiffness of a layered solid can be expressed by an 'effective modulus' E_e^*, which has been deduced from the experimental measurements and compared with the theoretical values with fair success. The work of adhesion is commonly measured in the SFA by observing the 'pull-off force' to separate the surfaces. The theory shows that, for a layered solid, the pull-force can vary significantly from the JKR value for a homogeneous solid. In particular, it was found that the mica surface energy, γ_{sv}, measured by SFA experiments using crossed cylinders of mean radius R, where the materials are layered and the mica/mica adhesion is high, can vary with the pull-off force F_p according to $F_p/4\pi R < \gamma_{sv} < F_p/2\pi R$, and for this particular experiment was given as $\gamma_{sv} = F_p/3.5\pi R$ as compared with $\gamma_{sv} = F_p/3\pi R$ for homogeneous materials.

1. Introduction

Understanding the mechanical properties of materials often requires knowledge of the contact deformation mechanisms of that material. The deformation of a solid is a function of the applied force, elastic and plastic properties of the solid, surface roughness and surface energy [1–3]. The degree of deformation leads to information about the strength, compliance, and adhesion of materials [3]. For example, the bulk properties of ceramic materials depend upon the nature of the solid/solid interaction of the grains within the ceramic

[6] Official contribution of the National Institute of Standards and Technology; not subject to copyright in the United States.

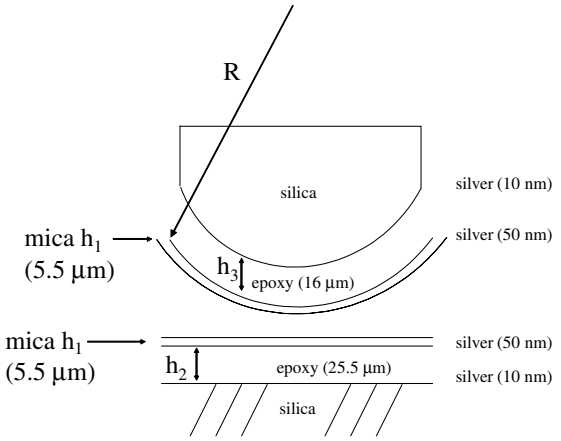

Figure 1. Schematic diagram of the layered mica/epoxy/silica system. The two mica surfaces were brought into contact and the contact radius was measured. The epoxy thicknesses were measured from the secondary interference fringe pattern obtained from light reflected from the 10 and 50 nm silver layers. The mica thickness and contact radius were measured from light reflected from the two 50 nm silver layers.

and the resulting deformations [3]. The multilayer structure of these experiments is similar to many biomaterials such as teeth that consist of a top enamel coating layer and a compliant tooth dentin layer underneath. Understanding the mechanics of model systems such as that described here could aid in the development of superior prosthetic devices.

Hertz first proposed the theory of contact between two elastic solids in 1881 [1, 4]. No interaction was assumed to occur between the solids except a hard core wall repulsion at contact. Hence, the surfaces would separate at zero force. Johnson, Kendall and Roberts (JKR) modified the Hertz interaction energy to include surface energy in the interaction and predicted a greater contact size at a fixed force than that found from Hertz theory due to the contributions of surface and interface energies [5]. JKR theory assumes the material to be homogeneous, isotropic and perfectly elastic and is applicable when the elastic deformation caused by the surface forces is large compared with the range of the surface forces.

JKR theory has been successfully used to model the adhesion between rubber elastomeric hemispheres [6]. In these experiments, an optical microscope measured the flattened contact radius as a function of the applied force as two spherical elastomeric hemispheres contact. More recently, polymers and self-assembled monolayers have been attached to polydimethylsiloxane (PDMS) hemispheres to allow the interaction of a variety of materials to be measured [7]. The low bulk modulus of the PDMS hemisphere is expected to dominate the mechanical response of the system whereas the thin coating would determine the surface properties.

Another technique used to directly measure the properties of surfaces is the surface forces apparatus (SFA) [8]. Typically, two thin molecularly smooth mica sheets are bonded via an epoxy layer to cylindrical silica lenses and are brought into contact with the cylinder axes perpendicular to one another (figure 1). This geometrical configuration is equivalent to contact of a sphere on a flat. Optical interference fringes are used to measure the amount of surface deformation at the point of contact and the contact radius as a function of the applied force. Previous measurements of the deformation of the surfaces showed a trend consistent with JKR theory, but JKR theory underestimated the measured contact radius by as much as 30% [9]. A more recent measurement under sliding conditions showed better agreement [10]. However, JKR theory assumes homogeneous, isotropic surfaces, which is not the case for the layered materials of the SFA experiments.

A finite element analysis (FEA) of the SFA geometry on which this paper is based was presented by Sridhar *et al* [11]. In that paper the concept of an effective modulus of elasticity, E_e^* was introduced. It is defined as the modulus of a homogeneous solid which has the same contact stiffness as the layered solid. Clearly, the value of E_e^* depends on the thickness and moduli of the individual layers. When normalized by the modulus of, say, the surface layer, E_1, the ratio E_e^*/E_1 provides a meaningful non-dimensional measure of the variation in contact stiffness with depth of deformation. In the case of the SFA for very small forces, the deformation will be contained in the mica layer and will be approximated by the mica modulus, E_1. As the contact size increases with increasing force, E_e^* of the system will be increasingly influenced by the epoxy layer and eventually the silica substrate. The extended theory predicts that the contact radius–force dependence for a layered system has the same general JKR curve shape as that found in a homogeneous isotropic sample. The adhesion characteristics, including the pull-off force, are found to depend upon an adhesion parameter, α, as well as on the mica and epoxy layer thicknesses and their elastic moduli. However, because the layer thicknesses and moduli were not measured in previous SFA experiments, a direct comparison of the theory to experiments for layered materials was not obtained.

In the present experiments, the elastic moduli of mica and epoxy are measured by nanoindentation and microindentation, respectively, using spherical indenters. Nanoindentation is also used to obtain the effective modulus of a layered mica/epoxy material. The SFA is then used to measure the adhesion and deformation of two thin mica sheets which are attached to cylindrical silica supports with an epoxy layer. The mica thickness, h_1, epoxy thicknesses, h_2 and h_3, as well as the contact radius, a, as a function of applied force in adhesive and non-adhesive contact, are also measured by optical interferometry at the point of contact. By measuring all the experimental parameters, the validity of using the modified JKR theory for a layered structure is experimentally examined.

2. Theory

For homogeneous materials, a number of theories have been derived to investigate the indentation and adhesion between two surfaces [5, 12–15]. The theories generally apply only within certain limits. As previously mentioned, JKR theory is applicable when the elastic deformation caused by the surface forces is large compared with the range of the surface forces. This condition is satisfied when the Tabor parameter μ is greater than 5 and is given by [16]

$$\mu \equiv \left(\frac{Rw^2}{E_e^{*2} z_o^3}\right)^{1/3}, \qquad (1)$$

where R is the mean radius of the crossed cylinders, E_e^* is the effective elastic modulus, z_o is the equilibrium separation of

the surfaces and w is the work of adhesion. For the layered mica surfaces used in the SFA measurements reported here, $R = 2.64\,\text{cm}$, $w = 120$–$200\,\text{mJ m}^{-2}$, $E_e^* \approx 30 \times 10^9\,\text{Pa}$ and $z_o \approx 0.3\,\text{nm}$, giving $\mu \approx 35$; the JKR theory can be applied to these measurements.

For layered materials, there have been many treatments of the contact and indentation of an elastic layered solid, both with and without adhesion between the surfaces [17–25]. We shall make use of the numerical finite element approach developed for the specific purpose of analysing the SFA system described above [11]. The principal features of the theory will be outlined here.

According to the JKR theory, the relationship between the net contact force, F, and the contact radius, a, between two elastic homogeneous spheres of radius R_1 and R_2 is given by [5]

$$F = F_o - F_a = \frac{4E_e^* a^3}{3R} - \sqrt{8\pi a^3 w E_e^*}, \tag{2}$$

where $1/R = 1/R_1 + 1/R_2$, E_e^* is the effective modulus of the two spheres and is given by $1/E_e^* = (1-\nu_1^2)/E_1 + (1-\nu_2^2)/E_2$, where E_1 and E_2 are the modulus of each sphere and υ_1 and υ_2 are their respective Poisson's ratio and w is the work of adhesion which, for identical surfaces is twice the surface energy, $2\gamma_{sv}$. F_o and F_a correspond to the applied Hertz force (no adhesion) and the adhesive (flat punch) force, respectively. In the absence of adhesion, the force reduces to F_o, the Hertz value. It follows from equation (2) that for adhesive contact when $F = 0$, the contact radius is given by

$$a_0^3 = \frac{9\pi R^2 w}{2E_e^*} \tag{3}$$

and the surfaces separate at the 'pull-off' force, F_p, where $\partial F/\partial a = 0$ and is given by

$$F_p = -\frac{3\pi R w}{2}. \tag{4}$$

Rearranging equation (4) shows that the normalized pull-off force, $F_p/3\pi Rw$, is a constant -0.5 for a homogeneous system obeying JKR mechanics. The JKR theory as detailed can be considered locally as a rigid sphere of radius R indenting an elastic half-space.

This homogeneous JKR theory has been extended for a surface consisting of two layers on a substrate indented by a rigid sphere using FEA. The Hertz force and adhesive force terms in equation (2) are evaluated separately. The contribution of the normalized Hertz force F_o may be written in a generalized non-dimensional form as

$$\frac{F_o R}{E_1' a^3} = f\left\{\frac{a}{h_1}, \frac{h_2}{h_1}, \frac{E_2'}{E_1'}, \frac{E_3'}{E_1'}\right\} \tag{5}$$

and the normalized adhesion (flat punch) term F_a may be written in a generalized non-dimensional form as

$$\frac{F_a}{\sqrt{2E_1' w a^3}} = g\left\{\frac{a}{h_1}, \frac{h_2}{h_1}, \frac{E_2'}{E_1'}, \frac{E_3'}{E_1'}\right\}, \tag{6}$$

where h_1 and h_2 are the thicknesses of the mica and epoxy layers and E_1', E_2', E_3' the plane-strain elastic moduli of the mica and epoxy layers and the glass substrate, respectively. The plane-strain modulus E_i' is defined as $E_i/(1-\upsilon_i^2)$, where υ_i is the Poisson's ratio of the respective layers. Knowing the values of the thicknesses and moduli, f and g are computed as functions of the normalized contact radius, (a/h_1) [11,26]. Substituting equations (5) and (6) into (2) and rearranging gives

$$\begin{aligned}\frac{FR}{E_1' a^3} &= \frac{F_o R}{E_1' a^3} - \left(\frac{2wR^2}{E_1' h_1^3}\right)^{1/2}\left(\frac{h_1}{a}\right)^{3/2}\frac{F_a R}{E_1' a^3} \\ &= f\left(\frac{a}{h_1}\right) - \alpha\left(\frac{h_1}{a}\right)^{3/2} g\left(\frac{a}{h_1}\right),\end{aligned} \tag{7}$$

where the quantity $FR/E_1' a^3$ is termed the normalized force and α is the adhesion parameter which can be considered as a non-dimensional measure of the work of adhesion and is defined by

$$\alpha \equiv \left(\frac{2wR^2}{E_1' h_1^3}\right)^{1/2}. \tag{8}$$

The general shape of the interaction curve for layered materials obtained from equation (7) is similar to that of the JKR curve for homogeneous materials [11]. The pull-off force F_p is the minimum (maximum negative) value of F expressed in equation (7) and is dependent on the adhesion parameter, α.

The non-adhesive Hertz deformation for a layered system can be measured by indentation. In most indentation experiments it is difficult to measure the contact radius, whereas indentation depth can be easily monitored with displacement measuring transducers. The indentation depth d_o can be written in a generalized non-dimensional form as

$$\frac{d_o R}{a^2} = B\left\{\frac{a}{h_1}, \frac{h_2}{h_1}, \frac{E_2'}{E_1'}, \frac{E_3'}{E_1'}\right\}. \tag{9}$$

The function B has the value unity for Hertz deformation in a homogeneous material and in a layered material, its values are obtained from FEA. The function B can be used to determine the contact radius for a particular indentation depth. In order to calculate the contact radius, the function $B = d_o R/a^2$ is converted to $B^* = d_o R/h_1^2$ by multiplying B by $(a/h_1)^2$. At a specific indentation depth, B^* is determined and $a(d_o)$ is obtained from a graph of B^* versus a/h_1. Hence, a 'true' value of a can be found from the values of B^* (a/h_1). It is to be noted that, for the case of a single layer, $h_2 = 0$ and $E_3' = E_2'$ in equations (5), (6) and (9).

The 'effective modulus', E_e^*, of a layered solid is defined as the modulus which would give rise to the same stiffness, S, as a homogeneous solid. Thus

$$E_e^*(a) \equiv S(a)/2a, \tag{10}$$

where $S = \partial F_o/\partial d_o$. The stiffness S is determined experimentally by the derivative of the force-depth indentation data or theoretically from the finite element computations of indentation of a layered solid.

3. Experimental details

The SFA uses two molecularly smooth mica sheets bonded to silica cylindrical lenses with Epon™ 1004 epoxy (Shell Chemical Company, Houston, TX). In both the SFA

Table 1. The parameter values used in FEA calculations.

Layer material	Young's modulus (GPa)	Poisson's ratio	Layer thickness (μm)	Indenter radius (cm)
Mica	62	0.21	5.5	2.6
Epoxy	3.4	0.495	20	
Silica	72	0.25	—	

and indentation experiments, the Epon 1004 was heated above the melting point to allow spreading. In the melt state, Epon is viscous and readily wets both the glass and silvered mica surface. On cooling, the Epon 1004 acts to hold the mica onto the glass. Since we are only heating the Epon 1004 above the melting point during the preparation and no chemical crosslinkers are added, we assume that the measurements made at 23 °C are independent of the initial heating.

A 10 nm thick silver film was first sputtered onto the silica cylinders and the hot melt epoxy was spread onto the silvered cylinders. Mica sheets with 50 nm silver films on the back (epoxy) side were bonded with the epoxy to each lens. The cylindrical lenses are mounted in the SFA with their cylinder axes at right angles, producing a contact that is geometrically equivalent to a sphere on a flat. Figure 1 shows the geometry of the layered surfaces used in the SFA experiments.

The mica thickness, h_1, epoxy thicknesses, h_2 and h_3, contact radius, a, and cylinder radius, R, were all measured using multiple beam optical interferometry. Optical interference between the two 50 nm silver layers produced primary fringes of equal chromatic order allowing measurement of the mica thickness, h_1. In these experiments, the mica thickness was the same for each surface and was measured to be $h_1 = 5.5 \pm 0.1\,\mu$m. Interference between the 10 nm silver layer and the 50 nm silver layer produced secondary fringes, allowing measurement of the epoxy thickness, h_2 and h_3, at the point of contact. For this particular experiment, h_2 and h_3 were measured to be $25.5 \pm 1.5\,\mu$m and $16 \pm 1\,\mu$m, respectively. All measurements are summarized in table 1.

The radii of curvature of the mica surfaces, measured when the cylinders were not in contact, were determined from the shape of the primary interference fringes. For crossed cylinders, the radius is calculated from the geometric mean of the two cylinder radii, given by $R = (R_1 R_2)^{1/2} = 26 \pm 1.5$ mm [2]. The contact radius, a, was measured directly from the amount of flattening of the deformed primary fringes. The measured contact radii a were such that $5 \leqslant a/h_1 \leqslant 15$. Prior to each measurement, the contact is scanned and the maximum flattening (deformation) is recorded as the contact radius.

The lower cylinder was mounted on a double-cantilever spring which was used to apply a force to the crossed cylinders. The force was determined by measuring the deflection of the spring, which had a spring constant of $(1.2 \times 10^5) \pm (0.2 \times 10^5)\,\mathrm{N\,m^{-1}}$. Unless otherwise noted, the $\pm$ refers to the standard uncertainty in the measurements and is taken as one standard deviation of the observed values. Testing was performed in the closed chamber of the SFA which was purged with dry N_2 for at least 20 min prior to beginning the measurements. Solid P_2O_5 was placed in the chamber to ensure a dry atmosphere.

The SFA experiments were performed by bringing the mica surfaces into van der Waals contact at zero applied force. The force was increased in a step-wise fashion and the contact radius was measured. The measurements continued until an applied compressive force of approximately 500 mN was reached. The force was then decreased in a step-wise fashion with contact diameters being measured at each force until the surfaces spontaneously separated ('pull-off') at a negative (tensile) force, F_p. The time between loading steps was approximately 1 min, for a total loading/unloading time of approximately 40 min with 6–12 h between subsequent runs. All measurements were made at 23 °C.

Experimental details of the indentation experiments are given in the results section.

4. Results

4.1. Indentation of bulk materials

4.1.1. Mica. The bulk elastic properties of the mica used in the experiment were measured by instrumented nanoindentation tests that were performed on a rigidly supported 500 μm thick piece of mica. A commercial nanoindenter (Nano Indenter II, Nano Instruments, Inc.) was used to record force and displacement as a 21 μm radius spherically tipped diamond indenter was loaded onto the mica surface. A range of forces from 1 to 90 mN resulted in indentation depths from <20 nm to approximately 350 nm. All displacement was elastic; the mica did not deform permanently even at the highest forces and no residual impressions were observed. A Hertzian analysis of this elastic sphere-on-flat contact permits the determination of the quantity $E_1' = E_1/(1-\nu_1^2)$, where ν_1 is the Poisson's ratio for mica, assuming that the material is elastically isotropic. Although the isotropic assumption is not likely to be true for a material with mica's layered structure, the indentation experiment applies force along the same axis (perpendicular to the planes of the layers) as in the surface force experiments, and thus can be considered valid. The value obtained for $E_1/(1-\nu_1^2)$ for mica by this technique was 65 ± 1 GPa. Although ν_1 could not be independently determined, it is likely to fall in the range $0.15 \leqslant \nu_1 \leqslant 0.25$ for a covalently bonded oxide, giving a value of $E_1 = E_{\mathrm{mica}} = 62 \pm 2$ GPa. The value of E_{mica} is consistent with previous Brillouin scattering measurements [27].

4.1.2. Epoxy. The bulk elastic properties of the epoxy ($E_2 = E_{\mathrm{epoxy}}$) were measured using an instrumented microindenter. Epon 1004 epoxy was preheated in a vacuum oven overnight to remove residual air bubbles and a thick epoxy layer (>2 mm) was directly applied onto a solid sample stub. The Epon 1004 was cooled to room temperature before the measurement. The epoxy was indented with a 2.38 mm diameter tungsten carbide sphere with a loading rate of approximately $0.5\,\mathrm{N\,s^{-1}}$ to a maximum force of 5 N, a 5 s hold at peak force and an unloading rate of approximately $1\,\mathrm{N\,s^{-1}}$. The indentation is assumed to follow Hertz theory and the elastic modulus was calculated from the force—depth data using a linear least squares fit of the $F^{2/3} - d_o$ data [28] (approximately 200 points) assuming $\nu_2 = 0.5$. The force–depth curve of the epoxy closely followed Hertz contact theory

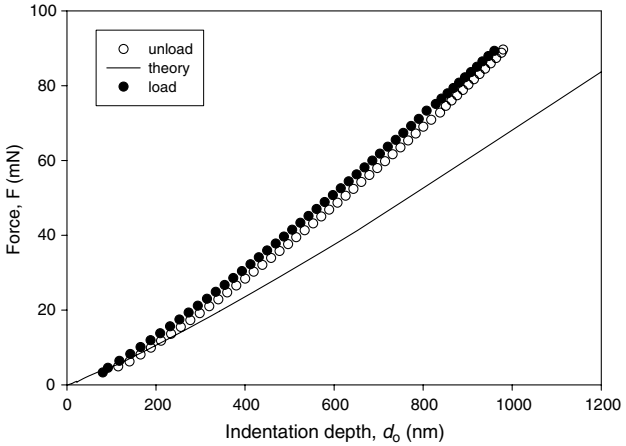

Figure 2. Non-adhesive Hertz contact for a two layer material: Nanoindentation measurements of the indentation depth d_o with applied force F during indentation of a 5.5 μm layer of mica on a thick epoxy substrate by a 21 μm radius diamond sphere. The solid circles represent load measurements whereas the open circles represent unload measurements. The solid line shows finite element calculations for layered surfaces.

and a negligible loading/unloading hysteresis was present. The maximum indentation depth was 8.4 μm for a 5 N force. Twenty five repeat measurements at different contact positions gave $E_2 = E_{\text{epoxy}} = 3.4 \pm 0.04$ GPa.

4.1.3. Silica. The Young's modulus, $E_3 = E_{\text{silica}}$, for the cylindrical silica supports is taken from the literature to be 72 ± 1 GPa [28].

4.2. Measurements of layered materials

4.2.1. Nanoindentation of a mica layer on a thick epoxy substrate: non-adhesive contact. Nanoindentation was used to measure the effective modulus of a mica layer on a thick epoxy substrate. Mica of the same thickness used in the SFA ($h_1 = 5.5\,\mu$m) was bonded to a silica substrate using a thick layer of the epoxy ($h_2 > 100\,\mu$m) and the system was indented with a 21 μm radius diamond sphere. At indentation forces <20 mN, the indentation process was entirely elastic; neither the mica nor the epoxy underwent any permanent deformation, as evidenced by the absence of hysteresis in the loading/unloading cycle. At a maximum force of 90 mN, a small amount of hysteresis was present, as shown by the slight difference between the load/unload curves in figure 2. The solid line in figure 2 is the prediction from FEA and will be discussed later.

4.2.2. SFA measurements: non-adhesive contact. In order to determine the contact behaviour of the mica surfaces when adhesive forces were absent, a droplet of 10^{-3} mol L^{-1} KCl solution was placed between the mica surfaces. The interaction between mica surfaces immersed in an aqueous 10^{-3} mol L^{-1} KCl solution is repulsive due to a short range hydration force, thus the interaction is expected to follow Hertz contact mechanics, as opposed to JKR contact mechanics [29]. No adhesion was measured between the surfaces in the 10^{-3} mol L^{-1} KCl solution, i.e. the surfaces separated when

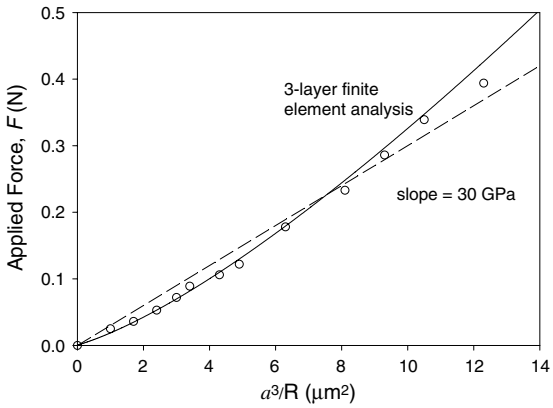

Figure 3. Non-adhesive Hertz contact for a three layer material: SFA measurements of applied force F versus a^3/R for one unloading run in 10^{-3} mol L^{-1} KCl solution (non-adhesive Hertz contact). The dashed line is a least squares fit to the data and is expected from homogeneous Hertz theory. The solid curve is the FEA of the Hertz contact predicted for a 3-layer system.

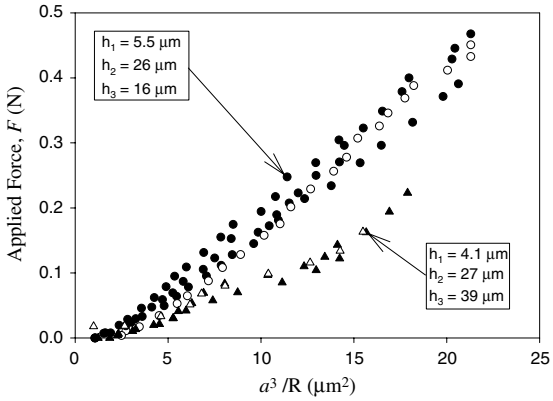

Figure 4. Comparison of the (non-adhesive) Hertz contact between mica surfaces interacting in 10^{-3} mol L^{-1} KCl solution for two SFA experiments. The epoxy and mica thicknesses were different for each experiment and are given on the graph. The triangles and circles represent measurements for an average epoxy thickness of 33 μm and 20 μm, respectively. The filled and open symbols represent load and unload measurements, respectively.

the applied force was reduced to zero, as expected from Hertz contact theory.

Figure 3 shows the results of applied force F versus a^3/R for one unloading run in 10^{-3} mol L^{-1} KCl solution. If each of the contacting solids was homogeneous with an effective modulus E_e^*, Hertz theory predicts a linear relationship with slope of $4E_e^*/3$ as shown by the dashed line in figure 3. The upward curvature of the experimental data shows that E_e^* is not constant, but increases with depth of indentation as the stiffness of the silica substrate is increasingly felt. The solid line is the FEA for 3-layer surfaces and predicts the increase of E_e^* as measured. The shape of the contact zone under compressive force in non-adhesive contact is more rounded (less defined) at the edges than in adhesive contact. As a result, the radius of contact is less distinct in non-adhesive contact and could only be measured to within $\pm 10\%$, with even more uncertainty at small contact radii.

Repeat measurements of the variation of the contact radius with force in 10^{-3} mol L^{-1} KCl solution are shown

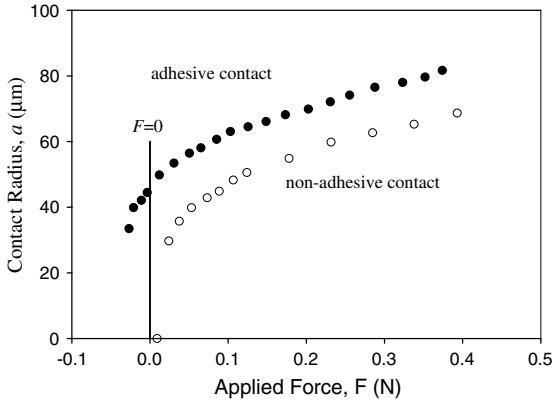

Figure 5. SFA measurements of the contact radius versus applied force for mica surfaces interacting in air (adhesive contact, filled circle symbols) and 10^{-3} mol L^{-1} KCl solution (non-adhesive contact, open circle symbols). The data were taken from unloading measurements. Note the larger contact diameter at a given force for the adhesive contact than for the non-adhesive contact. The same contact position was used for both sets of measurements. The contact radius is measured to ±5%.

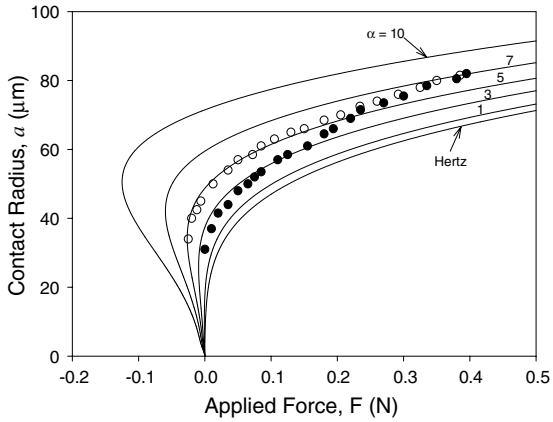

Figure 6. Adhesive contact: SFA measurements of the contact radius a as a function of applied force F for mica surfaces interacting in dry air. The filled circles are for loading measurements whereas the open circles are for unloading measurements. The contact radius is measured to ±5%. The solid lines are the FEA calculations of the 3-layer analysis for a range of values of the non-dimensional adhesion parameter $\alpha = (4\gamma_{sv}R^2/E_1h_1^3)^{1/2}$.

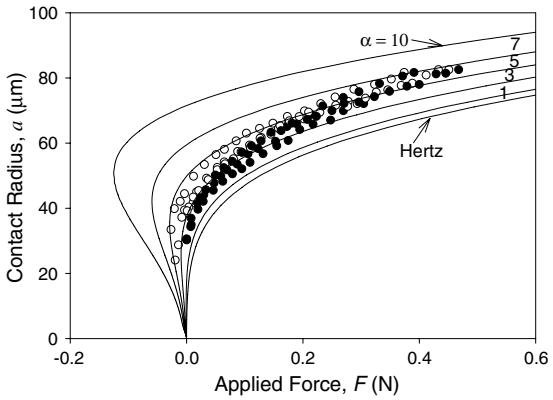

Figure 7. Adhesive contact: repeat SFA measurements of the contact radius a as a function of applied force F for mica surfaces interacting in dry air. The solid lines are the FEA calculations of the 3-layer analysis for a range of values of the non-dimensional adhesion parameter $\alpha = (4\gamma_{sv}R^2/E_1h_1^3)^{1/2}$. The filled and open symbols represent load and unload measurements, respectively.

in figure 4. The filled/open circles represent load/unload measurements for the conditions previously described ($h_1 = 5.5\,\mu$m, $h_2 = 25.5\,\mu$m and $h_3 = 16\,\mu$m). The filled/open triangles represent load/unload measurements from another experiment where the epoxy thickness was greater ($h_1 = 4.1\,\mu$m, $h_2 = 27\,\mu$m and $h_3 = 39\,\mu$m). Clearly, a larger contact radius is measured for the experiment with the larger epoxy thickness, as expected.

4.2.3. SFA measurements: adhesive contact. Figure 5 compares the measured contact radius, a, versus applied force, F, on loading for mica surfaces in dry N_2 (solid circles) and 10^{-3} mol L^{-1} KCl solution (open circles). The data represent measurements for the adhesive and non-adhesive cases, respectively, for the same experimental contact position where the mica and glue thicknesses are the same. As expected for the low forces used in these SFA experiments, the non-adhesive contacts have smaller radii at a given force than adhesive contacts.

Figure 6 shows measurements of the contact radius versus force in dry N_2 for loading (filled symbols) and unloading (open symbols). As seen in the figure, significant hysteresis is observed with a of the unloading curve greater than or equal to a of the loading curve. For the experimental force run shown in figure 6, the pull-off force on unloading gave $\gamma_{sv} = 100$ mJ m^{-2} using equation (4). The solid lines are the theoretical calculations for a 3-layer material given by equation (7) for various adhesion parameters and will be discussed later.

Repeat measurements of the contact radius during loading (filled circles) and unloading (open circles) at the same contact position are shown in figure 7. The solid lines are the theoretical calculations for a 3-layer material given by equation (7) for various adhesion parameters. The amount of hysteresis varied from run to run, indicating that the viscoelastic effects of the epoxy may be influencing the measured contact radius. The value of the zero force contact radius a_o taken on unloading had an 8% variation for different runs. However, there was less than 1% variation in the value of a_o measured on each subsequent loading curve after leaving the sample unloaded for 6 h or more. Since a_o on loading was similar for each run, no permanent gross plastic deformation of the epoxy occurred.

The range of pull-off force, F_p, for different runs was measured to be between −15 and −25 mN, corresponding to an interfacial energy, 60 mJ $m^{-2} \leqslant \gamma_{sv} \leqslant 100$ mJ m^{-2}, calculated using equation (4). For adhesive contact in a layered solid, the theoretical relationship between applied force F and contact radius a is given by equation (7) and depends on the adhesion parameter α (equation (8)). The values of γ_{sv} calculated from the pull-off experiments give $4 \leqslant \alpha \leqslant 5$.

5. Numerical results

The theory outlined above has been used to analyse the three experimental situations described in this paper: a thin (5.5 μm) mica layer bonded to a thick (>100 μm) layer of

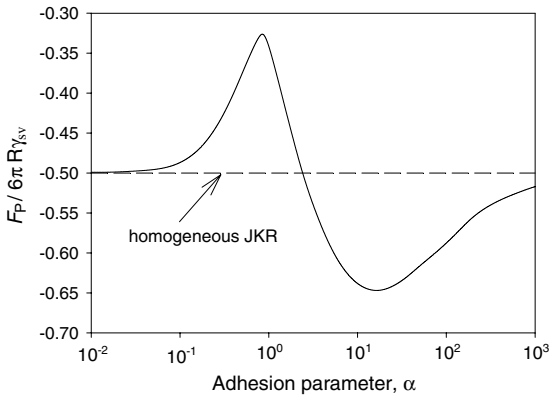

Figure 8. Adhesive contact: the solid curve shows results of finite element calculations of the non-dimensional pull-off force $F_p/6\pi R\gamma_{sv}$ as a function of the adhesion parameter $\alpha = (4\gamma_{sv}R^2/E_1h_1^3)^{1/2}$, for the three layered SFA configuration shown in figure 1 as predicted by the FEA analysis for layered materials. The dashed line at $F_p/6\pi R\gamma_{sv} = -0.5$ represents the analysis for a homogeneous material.

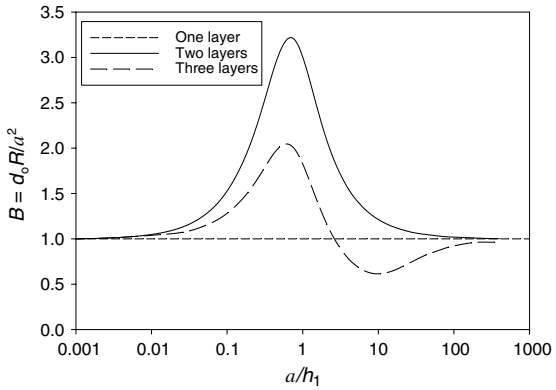

Figure 9. Non-adhesive Hertz contact: the computed relationship between contact radius a and indentation depth d_o expressed by the function $B\ (a/h_1) = (d_oR/a^2)$. The solid curve represents calculations for a 5.5 μm mica film on a thick epoxy substrate (2 layers) whereas the dashed curve represents calculations for the SFA system shown in figure 1 (3 layers). The dashed straight line at $B = 1.0$ corresponds to calculations for a homogeneous material (1-layer).

epoxy, and the SFA arrangement of layers of mica (5.5 μm), epoxy (20 μm) and silica, both with and without adhesion at the interface. The bulk material properties obtained from indentation and SFA measurements are summarized in table 1 and used as input values to the finite element simulation of the SFA and indentation experiments. The commercial finite element program ABAQUS was used to evaluate the functions f, g and B given by equations (5), (6) and (9). The calculation procedure is explained briefly in appendix A. Once the functions f and g were evaluated, the net force as a function of contact radius can be found for a given adhesion parameter using equation (7). A direct comparison of the theoretical calculations to experimental SFA measurements in adhesive contact is shown in figures 6 and 7. Using the thicknesses measured in the SFA experiments and the moduli measured by indentation, the computed values of the contact radius (equation (7)) are shown by the solid curves in figure 6 for a series of values of the adhesion parameter α (equation (8)) along with the experimental measurements (circles). The experimental measurements lie between $2 \leqslant \alpha \leqslant 7$, but the data do not follow the shape of the layered JKR predictions.

Repeat measurements of the adhesive contact radius during loading and unloading at the same contact position, including those shown in figure 6, are shown in figure 7. The solid lines are the theoretical calculations given by equation (7) for various adhesion parameters. All the experimental force curves in figure 7 lie between $2 \leqslant \alpha \leqslant 7$. However, the experimental data are not a good fit to the shape of the curve and fail to follow the expected increase in E_e^* at higher forces. It is noteworthy that the comparison shown in figures 6 and 7 does not involve any disposable parameters; the experiment is directly compared with theory. All the experimental runs showed a significant and variable amount of hysteresis, presumably due to viscoelastic effects in the epoxy layer at large contact indentations. In these circumstances, a close fit with a perfectly elastic theory would not be expected.

Computed values of the normalized pull-off force, $F_p/6\pi R\gamma_{sv}$, as a function of the adhesive parameter α are presented in figure 8. It can be seen that for a range of adhesion parameter values, for the current film thicknesses and moduli used in the measurements, the normalized pull-off force value can differ from the homogeneous JKR value of -0.5 by as much as 30%. For example, a value of α between 4 and 5 was calculated using equation (8) and the experimental pull-off force measurements. At $4 < \alpha < 5$, the computations suggest that $F_p/6\pi R\gamma_{sv} = -0.58$ as compared with $F_p/6\pi R\gamma_{sv} = -0.50$ in the homogeneous case (equation (4)). This important result will be discussed further in the discussion.

In non-adhesive contact, a direct comparison of finite element computations to indentation measurements is shown in figure 2. The computations predict a stiffer response than measured by indentation. The variation of the computed normalized indentation depth (without adhesion), described by the function B, with normalized contact radius (a/h_1) given by equation (9) is plotted in figure 9 for a mica layer on a thick epoxy substrate (solid curve), corresponding to a 2-layer nanoindentation configuration, and for mica and epoxy layers on a silica substrate (dashed curve) for the 3-layer SFA configuration. For reference, the computed values of the function B are listed in table 2. For small contact radius $(a/h_1 \leqslant 0.005)$ and large contact radius $(a/h_1 \geqslant 50)$ the value of function B is equal to 1. For intermediate values of the contact radius, $0.005 < a/h_1 < 50$, $1 < B < 3.2$ for the two layer case. In the 2-layer case (curved solid line in figure 9), for $a/h_1 = 1$, $B = 3.2$, $a = ((d_oR)/3.2)^{1/2}$, the 'true' contact radius is 56% smaller than the homogeneous Hertz radius. Note that in the homogeneous Hertzian case, $a = \sqrt{d_oR}$, thus $B = d_oR/a^2 = d_oR/((d_oR)^{1/2})^2 = 1$. This is shown by the straight dashed line at $B = 1$ in figure 9. Similar indentation analysis for coated materials has been previously reported [17].

For the SFA (3-layer) geometry (dashed curve, figure 9), in the practical range of normalized contact radii of $10^{-3} < a/h_1 < 500$, the function B varies from 0.6 to 2.1.

The theoretical variations of the effective modulus E_e^* versus normalized contact radius (a/h_1) are shown by the solid line in figure 10 for the nanoindentation configuration of a mica layer on a thick epoxy substrate (2 layers) and in

Table 2. The computed values for function $B(a/h_1) = d_o R/a^2$ from FEA.

a/h_1	$B(a/h_1) = d_o R/a^2$ for two layers	$B(a/h_1) = d_o R/a^2$ for three layers
0.001	1	1
0.01	1.048 0295	1.039 1843
0.02	1.099 8835	1.059 6785
0.05	1.260 099	1.142 6278
0.07	1.366 0897	1.197 4301
0.1	1.527 2775	1.281 557
0.2	2.030 2227	1.539 4609
0.4	2.830 7013	1.921 5777
0.7	3.218 5252	2.029 7194
1	3.004 7525	1.825 6835
1.4	2.582 3243	1.515 158
1.75	2.290 3748	1.308 304
2.5	1.903 009	1.032 6499
3.25	1.688 2351	0.879 166 96
5	1.439 0059	0.708 871 94
7	1.308 9621	0.637 525 16
10	1.213 2741	0.614 241 48
15	1.140 0252	0.642 955 98
20	1.104 089	0.687 268 42
40	1.050 9653	0.811 880 64
60	1.033 0039	0.866 762 91
80	1.022 6873	0.901 991 25
100	1.018 8411	0.921 834 29
200	1.008 6244	0.961 212 22
400	1.001 8156	0.978 250 96

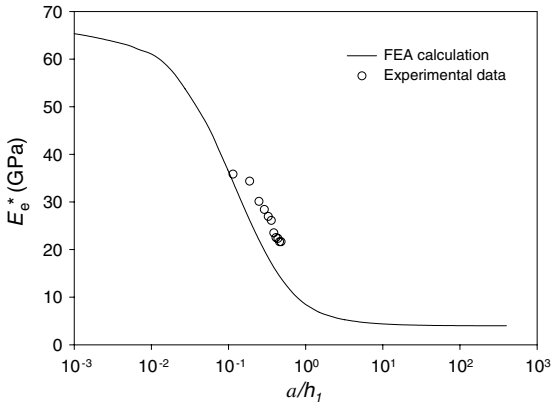

Figure 10. Variation of the effective modulus E_e^* of a solid comprising a 5.5 μm mica layer on a thick epoxy substrate as a function of the contact radius, a/h_1. The solid line is the finite element calculation for a 2-layer material and the circles represent measured values extracted from nanoindentation tests with a 21 μm radius diamond sphere (figure 2).

figure 11 for the SFA configuration (3 layers). As shown in figure 10, the calculated effective modulus, E_e^*, of the 2-layered system decreases steadily from the modulus of the mica (62 GPa) to that of the epoxy (3.4 GPa) as the size of the contact increases relative to the thickness of the mica layer (5.5 μm). Equation (10) can be used to directly compare the theoretical computations to the experimental indentation measurements. The indentation stiffness $S(d_o)$ is obtained from the differentiation of the indentation curve in figure 2. However, the variation of the radius of contact a with indentation depth is required to obtain the effective modulus E_e^* from equation (10). Since a cannot be directly measured in nanoindentation experiments, $a(d_o)$ is obtained from the

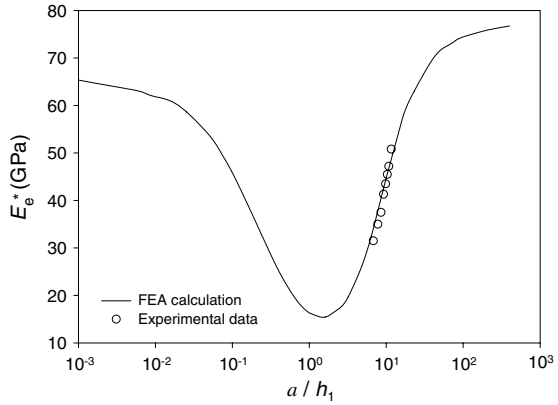

Figure 11. Variation of the effective modulus E_e^* of the layered solids in the SFA as a function of a/h_1. The solid line is the finite element calculation of the 3-layer material (5.5 μm mica layer, 20 μm epoxy layer, and infinite silica layer) and the circles represent measured values extracted from the SFA tests in the absence of adhesion (figure 3).

computed function $B(a/h_1)$ (equation (9) and figure 9). By converting the function $B = d_o R/a^2$ to $B^* = d_o R/h_1^2$ (by multiplying B by $(a/h_1)^2$), a 'true' value of a can be found from the values of $B^*(a/h_1)$. The values of $B(a/h_1)$ are given in the appendix. Values of E_e^* so found are added to figure 10 (open circles), where they are compared with the computed results (solid curve). There is a discrepancy between the measured and theoretical absolute values of E_e^*, but the trend clearly shows the increasing effect of the epoxy as the depth and area of the indentation increases. The discrepancy suggests that the value of the modulus of the mica or the epoxy is too low. Using the function $B(a/h_1)$, the contact radius and modulus for a particular indentation depth can also be calculated. At an indentation depth of 30 nm on a 5.5 μm mica layer, the calculations show that $a/h_1 = 0.115$. From figure 10, at $a/h_1 = 0.115$, $E_e^* \sim 36$ GPa compared with the mica modulus of $E_{mica} = 62$ GPa. The indentation is sensing the epoxy layer at nearly 200 times the indentation depth and nearly 9 times the contact radius.

The calculated effective modulus of the SFA configuration consisting of a 5.5 μm mica layer and a 20 μm epoxy layer on a silica substrate, shown in figure 11, is more complex. For contact radii much smaller than the thickness of the mica layer, the effective modulus falls with increasing contact radii from the modulus of the mica, as seen in figure 10. For values of a/h_1 greater than about unity, the effective modulus increases due to the stiffening effect of the silica substrate. For values of $a/h_1 \approx 1$, the effective modulus is approximately constant with $E_e^* \approx 15$ GPa, and the system should behave according to the homogeneous JKR equation. Note that these results are only valid for the particular geometry and elastic constants (table 1) used in this experiment.

Experimentally, E_e^* for the layered SFA configuration can be determined from the non-adhesive force measurements and compared with theoretical calculations. The experimental values of E_e^* are found by converting the variation of force with a to variations with displacement d_o and hence the stiffness of the layered surface. It can be shown that $E_e^* = (3/4B)(\partial F/\partial(a^3/R))$. These experimental values of the effective modulus, shown by the circles in figure 11, compare

well with the theory. In addition, for the experimental contact radii $5 \leqslant a/h_1 \leqslant 15$, E_e^* increases with increasing force demonstrating the influence of the underlying silica surface. The increase in stiffness with increasing force is also noticed in figures 6 and 7 at larger contact radii.

6. Discussion

We shall consider first the indentation of layered solids without adhesion: (*a*) 5.5 μm mica layer on a thick epoxy substrate indented by a 21 μm radius diamond sphere and (*b*) a SFA configuration comprising a 5.5 μm mica and 20 μm epoxy layers on a glass substrate.

For the indentation of the two layer mica/epoxy by the diamond sphere, the variation of indentation depth with force was measured (figure 2) and the stiffness of the contact obtained from the derivative of this curve. The theoretical prediction is compared directly by the line in figure 2. It reveals an under-estimate of the contact stiffness by about 25%. The effective modulus E_e^* of the two layered solid was then obtained using the relation between contact radius and indentation depth shown in figure 9. These experimental values of E_e^* are compared with the numerical theory in figure 10. They follow the theoretical predictions of E_e^* with contact size and clearly show the increasing effect of the epoxy relative to the mica as the indentation depth increases. However, as expected from figure 2, the comparison between theory and experiment reveals a discrepancy in absolute value of about 25%. The SFA experiments without adhesion clearly show the increase in effective modulus E_e^* (figure 11) with increasing contact radius due to the effect of the silica substrate, in good agreement with the theory for layered materials.

However, the SFA experiments with adhesion shown in figures 6 and 7 are not so satisfactory. Loading/unloading tests show a significant and variable amount of hysteresis, presumably arising from viscoelastic effects in the epoxy layer. It is known that, with viscoelastic solids, adhesion on unloading is enhanced by the concentration of adhesive stress at the edge of the contact [24, 30]. Repeated SFA measurements showed that no permanent gross plastic deformation of the epoxy had occurred. The time scale between measurement runs was 6–12 h, and the epoxy appeared to relax within that time. However, during the time scale of one measurement load/unload curve (~45 min), hysteresis was observed. The microindentation experiments that were used to determine the elastic modulus of the epoxy were much faster (20–30 s), and showed minimal hysteresis or plasticity. It has been assumed that we are at equilibrium at each step during the SFA loading and unloading cycles, which may not necessarily be the case if the relaxation time is longer than the time scale of the experiments [12].

Some points of practical importance arise from this work. Firstly, it is common in JKR adhesion tests to extract a value for the surface energy from the measured pull-off force by equation (4) where $\gamma_{sv} = -F_p/3\pi R$. Note that in this equation the pull-off force depends solely on the mica surface energy and is independent of the contact dimension or modulus. But it is clear from figure 8 that, with a layered solid, using equation (4) can involve a significant error, and for this specific configuration, the surface energy varied according to $2\pi R\gamma_{sv} < F_p < 4\pi R\gamma_{sv}$, giving a variation of ±30%. The exact value of the pull-off force depends on the adhesion parameter α. For $\alpha = 5$, $F_p \approx -0.58$. Thus, $\gamma_{sv} \approx -F_p/3.5\pi R$. This result was found to be relatively independent of the layer thickness ratio h_2/h_1 [11]. It should also be noted that in a study of viscoelastic contact, it has been shown that the pull-off force can be significantly greater than the elastic JKR value [30].

Secondly, it is evident from figure 11 that when the scaled radius of contact, a/h_1, is near unity, the effective modulus is close to that of the epoxy. In the SFA case shown in figure 11, a minimum stiffness is found at $a/h_1 \approx 2$, after which it increases due to the stiffening effect of the silica substrate. In the region close to the minimum, E_e^* is approximately constant, independent of contact size, so that the JKR equation (equation (1)) could be applied to a good approximation. In the present SFA experiments with adhesion, shown in figures 6 and 7, the values of a/h_1 varied between 4.5 and 14. This is well outside the range of where E_e^* is approximately constant. However this is partly due to the use of a very high spring stiffness in the SFA used in these experiments.

Due to the large cylinder radius ($R \approx 2$ cm) and the thin mica sheets ($h_1 < 6\,\mu$m) typically used in SFA experiments, combined with the soft epoxy under-layer, the contact radius in air at zero force is generally 5 times greater than the mica layer thickness. Hence, the mica plays a minimal role in the overall measured mechanical properties of the SFA system; the mechanical properties are mostly dictated by the epoxy and the underlying silica surface, depending on the applied force.

It is often difficult to completely match theoretical and experimental conditions. This difference can allow the theoretical and experimental measurements to differ. For example, the experimental SFA measurements consist of two deforming surfaces (sphere-on-flat geometry) having epoxy thicknesses of 16 and 25 μm. The theoretical calculations model this contact as a rigid probe pressed onto a 3-layer material having an epoxy thickness of 20 μm, the average value of the two epoxy thicknesses. This averaging may lead to the slight differences between the experimental and theoretical values. In addition, the experimental measurement of the contact radius assumes the contact radius to be spherical, as is expected for crossed cylinders. However, if the cylinders were not at 90°, an elliptical contact would occur, and an error would exist in the measurements of the contact radius. Also, if the contact radii were not measured on a major axis, the measurements would further deviate from the theoretical predictions.

The results have implications for other experimental techniques, such as atomic force microscopy and nanoindentation, where the contact radius can vary from 5 to 1000 nm. Comparison of figures 10 and 11 show that even at very low contact radii ($10^{-2} < a/h_1 < 1$), the silica substrate is significantly influencing the measured modulus. For $a/h_1 = 0.01$ where there begins to be a difference between the response of a 20 μm epoxy layer thickness and an infinite epoxy thickness, $a = 0.55\,\mu$m. Hence, the silica is influencing the mechanical properties through 5.5 μm mica and 20 μm epoxy (26 μm of material), a distance that is approximately 25 times the contact diameter. These results show that even minute indentations

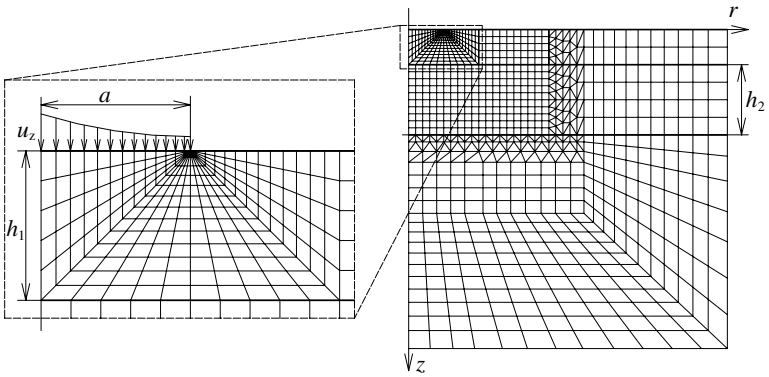

Figure A1. Finite element mesh for three layer SFA.

($a/h_1 > 10^{-2}$) can be influenced by the underlying materials and the measured effective modulus will be a composite response.

7. Conclusions

This paper reports an experimental investigation of the micro- and nanoindentation of layered surfaces. In particular, it investigates the contact mechanics of the SFA, both with and without adhesion. Almost all the parameters of the apparatus, the thickness and elastic modulus of the layers, are found by direct independent measurement. The experimental results are compared with a FEA of layered solids.

Nanoindentation of bulk mica gave the elastic modulus of mica: $E = 62 \pm 2$ GPa. Microindentation of bulk epoxy gave the modulus of epoxy: $E = 3.4 \pm 0.04$ GPa.

Indentation of a thin mica layer on an epoxy substrate gave values for the effective modulus E_e^* of a two layered solid. The variation of the effective modulus with depth of indentation agreed well with the layered Hertz theory, but the absolute magnitude was about 25% high. No satisfactory explanation has been found for this discrepancy.

SFA measurements in the absence of adhesion gave values for the effective modulus of the three layer configuration (mica and epoxy layers on a silica substrate) that were in good agreement with layered Hertz predictions, both in variation with depth and in absolute value.

In the presence of adhesion, SFA measurements of the contacting mica surfaces gave contact radius–force curves which were in reasonable agreement with the theory extended to layered materials. However, the loading and unloading curves showed appreciable adhesion hysteresis presumably due to viscoelasticity of the epoxy adhesive layer which prejudices comparison with an elastic theory. The FEA further showed that the pull-off force with a layered solid can vary significantly from the JKR value given by equation (3). Specifically, the analysis showed that $2\pi R\gamma_{sv} < F_p < 4\pi R\gamma_{sv}$ and for the experimental geometry of the SFA at the conditions of this experiment, $\gamma_{sv} \approx F_p/3.5\pi R$.

Acknowledgments

PMM would like to thank Jacob Israelachvili, Brian Lawn and Mark Robbins for their invaluable discussions.

Note: Certain commercial equipment, instruments or materials are identified in this paper in order to adequately specify the experimental procedure. Such identification does not imply recommendation or endorsement by the National Institute of Standards and Technology, nor does it imply that the materials or equipment identified are necessarily the best available for the purpose.

Appendix A. Numerical analysis

The function f and g are computed using commercial finite element (FE) package ABAQUS for a range of values of a/h_1. The finite element mesh for three layer SFA is shown in figure A1. All the layers are assumed to be perfectly bonded to each other. A large domain, 100–150 times the contact radius, is discretized using axi-symmetric 8-noded quadratic and 6-noded triangular elements. The hybrid elements are used to model the incompressible nature of the epoxy layer. A particularly fine mesh is required in the region close to the edge of contact radius $r = a$ in order to obtain reliable values of the stress intensity factor K_I. To simulate the spherical tip indentation, the normal displacement u_z is separated into two terms as

$$\frac{Ru_z}{a^2} = \frac{Rd_0}{a^2} - \frac{1}{2}\left(\frac{r}{a}\right)^2 \equiv \frac{Ru_z'}{a^2} - \frac{Ru_z''}{a^2}. \qquad \text{(A1)}$$

The stress arising from each displacement component are computed separately, and they give rise to stress intensity factors, K_I' and K_I'' at $r = a$. Summation of the nodal reaction forces on the surfaces gives the corresponding forces F' and F''. The adhesive force F_a is given directly by F'. In the absence of adhesion, the deformation is smooth at $r = a$, so that F_0 is given by the combination of F' and F'', which satisfies the condition $K_I' + K_I'' = 0$.

References

[1] Johnson K L 1982 *Proc. Inst. Mech. Eng.* **196** 363–78
[2] Johnson K L 1985 *Contact Mechanics* (Cambridge: Cambridge University Press)
[3] Lawn B 1993 *Fracture of Brittle Solids* 2nd edn (Cambridge: Cambridge University Press)
[4] Hertz H 1881 *J. Reine Angew. Math.* **92** 156

[5] Johnson K L, Kendall K and Roberts A 1971 *Proc. R. Soc. Lond. Ser* A *(Math. Phys. Sci.)* **324** 301–13
[6] Silberzan P, Perutz S, Kramer E J and Chaudhury M K 1994 *Langmuir* **10** 2466–70
[7] Chaudhury M K and Whitesides G M 1991 *Langmuir* **7** 1013–25
[8] Israelachvili J N and Adams G E 1976 *Nature* **262** 773–6
[9] Horn R G, Israelachvili J N and Pribac F 1987 *J. Colloid Interface Sci.* **115** 480–92
[10] Homola A M, Israelachvili J N, McGuiggan P M and Gee M L 1990 *Wear* **136** 65–83
[11] Sridhar I, Johnson K L and Fleck N A 1997 *J. Phys. D: Appl. Phys.* **30** 1710–19
[12] Maugis D and Barquins M 1978 *J. Phys. D: Appl. Phys.* **11** 1989–2023
[13] Derjaguin B V, Muller V M and Toporov Y P 1975 *J. Colloid Interface Sci.* **53** 314–26
[14] Barthel E and Haiat G 2002 *Langmuir* **18** 9362–70
[15] Shull K R 2002 *Mater. Sci. Eng. R—Rep.* **36** 1–45
[16] Tabor D 1977 *J. Colloid Interface Sci.* **58** 2–13
[17] Perriot A and Barthel E 2004 *J. Mater. Res.* **19** 600–8
[18] Hu X Z and Lawn B R 1998 *Thin Solid Films* **322** 225–32
[19] Doerner M F and Nix W D 1988 *CRC Crit. Rev. Solid State Mater. Sci.* **14** 225–68
[20] Gao H J, Chiu C H and Lee J 1992 *Int. J. Solids Struct.* **29** 2471–92
[21] Yoffe E H 1998 *Phil. Mag. Lett.* **77** 69–77
[22] Shull K R, Ahn D, Chen W L, Flanigan C M and Crosby A J 1998 *Macromol. Chem. Phys.* **199** 489–511
[23] Sergici A O, Adams G G and Muftu S 2006 *J. Mech. Phys. Solids* **54** 1843–61
[24] Mary P, Chateauminois A and Fretigny C 2006 *J. Phys. D: Appl. Phys.* **39** 3665–73
[25] Math S, Horn R, Jayaram V and Biswas S K 2007 *J. Colloid Interface Sci.* **308** 551–61
[26] Johnson K L and Sridhar I 2001 *J. Phys. D: Appl. Phys.* **34** 683–9
[27] Mcneil L E and Grimsditch M 1993 *J. Phys.: Condens. Matter* **5** 1681–90
[28] Oliver W C and Pharr G M 1992 *J. Mater. Res.* **7** 1564–83
[29] Pashley R M 1981 *J. Colloid Interface Sci.* **80** 153–62
[30] Johnson K L and Greenwood J A 2003 *Proc. 3rd Int. Symp. Contact Mechanics (CISM, Peniche, Portugal)* ed J A C Martins and M M Marques (Dordrecht: Kluwer)